

TADF/RTP OLED organic emitters based on concave N-PAHs with a tunable intrinsic D-A electronic structure

Jakub Wagner[‡], Paola Zimmermann Crocomo[‡], Michał Andrzej Kochman,[‡] Adam Kubas,^{*} Przemysław Data,^{*} Marcin Lindner^{*}

Institute of Organic Chemistry, Polish Academy of Sciences, Kasprzaka 44/52, 01-224 Warsaw, Poland;

Institute of Physical Chemistry, Polish Academy of Sciences, Kasprzaka 44/52, 01-224 Warsaw, Poland;

Silesian University of Technology, Faculty of Chemistry, Department of Physical Chemistry and Technology of Polymers, Strzody 9/208d, 44-100 Gliwice, Poland

[‡] these authors contributed equally

This paper is dedicated to Prof. Dr. Klaus Müllen on the occasion of his 75th birthday

KEYWORDS: PAHs, N-doping, Dyes/Pigments, Functional Aromatic Materials, RTP, TADF, OLEDs

ABSTRACT: The introduction of pyrrolic nitrogen dopants into the central sites of polycyclic aromatic hydrocarbons (PAHs) often gives rise to characteristic bowl-shaped structures due to the simultaneous introduction of 5- and/or 7-membered cycles. Although the incorporation of these heteroatoms achieves excellent electron-donating ability, the application of this strategy for the design of optoelectronics is hampered by typically low photoluminescence quantum yields (PLQYs). In order to address this issue, in the present study we report the synthesis and characterization of the first curved and fully conjugated nitrogen-doped PAHs in which an electronically diverse phenazine terminus serves as the electron-accepting moiety. We show that the curvature of the molecular skeleton increases the spatial separation between the HOMO and the LUMO, leading to low singlet-triplet gaps, which are essential for high reverse intersystem crossing (RISC) rates. Moreover, we evaluate the utility of the concave N-doped systems as TADF/RTP emitters, which has not been explored so far in the context of non-planar N-PAHs. By varying the electron-accepting ability of the phenazine terminus, we are able to tune the PLQY of the given compounds in a range from 9% to 86% (for a dinitrile substituted derivative). As a proof of concept, we constructed solid-state OLED devices exhibiting yellow to orange emission. The best-performing compound, built from a 3-(trifluoromethyl)phenyl decorated phenazine acceptor, shows a maximum external EL quantum efficiency (EQE) of 12%, which is the highest EQE in an curved D-A embedded N-PAH to date.

Polycyclic aromatic hydrocarbons (PAHs)^{1–3} unveiled within the last two decades have demonstrated an immense array of potential applications including as chemical sensors,⁴ organic field-effect transistors (OFETs),⁵ organic solar cells,⁶ fluorescence imaging labels,^{7,8} liquid crystals,^{9,10} and organic light-emitting diodes (OLEDs).¹¹ One of the most efficient approaches to rationally tune their physicochemical features is doping with elements other than carbon, either at the periphery of the molecule, or within the polyaromatic system. The dopant atoms alter both the electronic properties, such as the MO energy levels, and molecular geometry. The latter factor is of paramount importance for Nitrogen (N)-doped PAHs.^{12,13} A centrally positioned N-heteroatom surrounded solely by six-membered rings leads to various planar or only slightly bent architectures, such as the carbonyl, dimethyl, O, and S bridged N-heterotriangulenes, (Figure 1a, **1-4b**).^{14–17} Even though the latter examples prove to be strong electron donors, their modest thermal and morphological stability and high tendency towards π - π interactions impede their practical use.

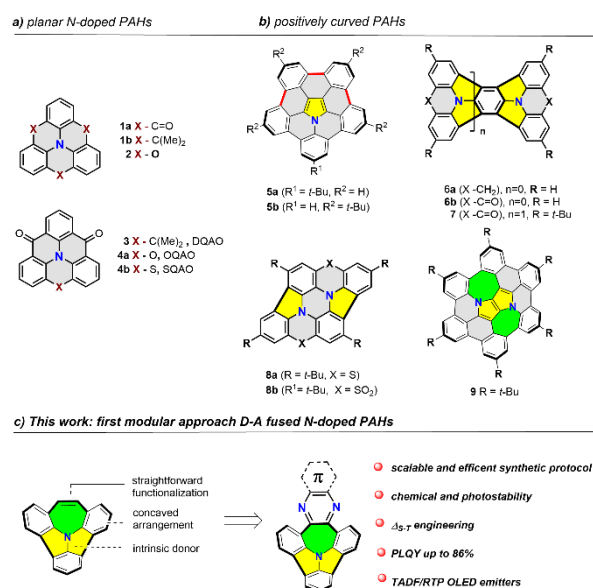


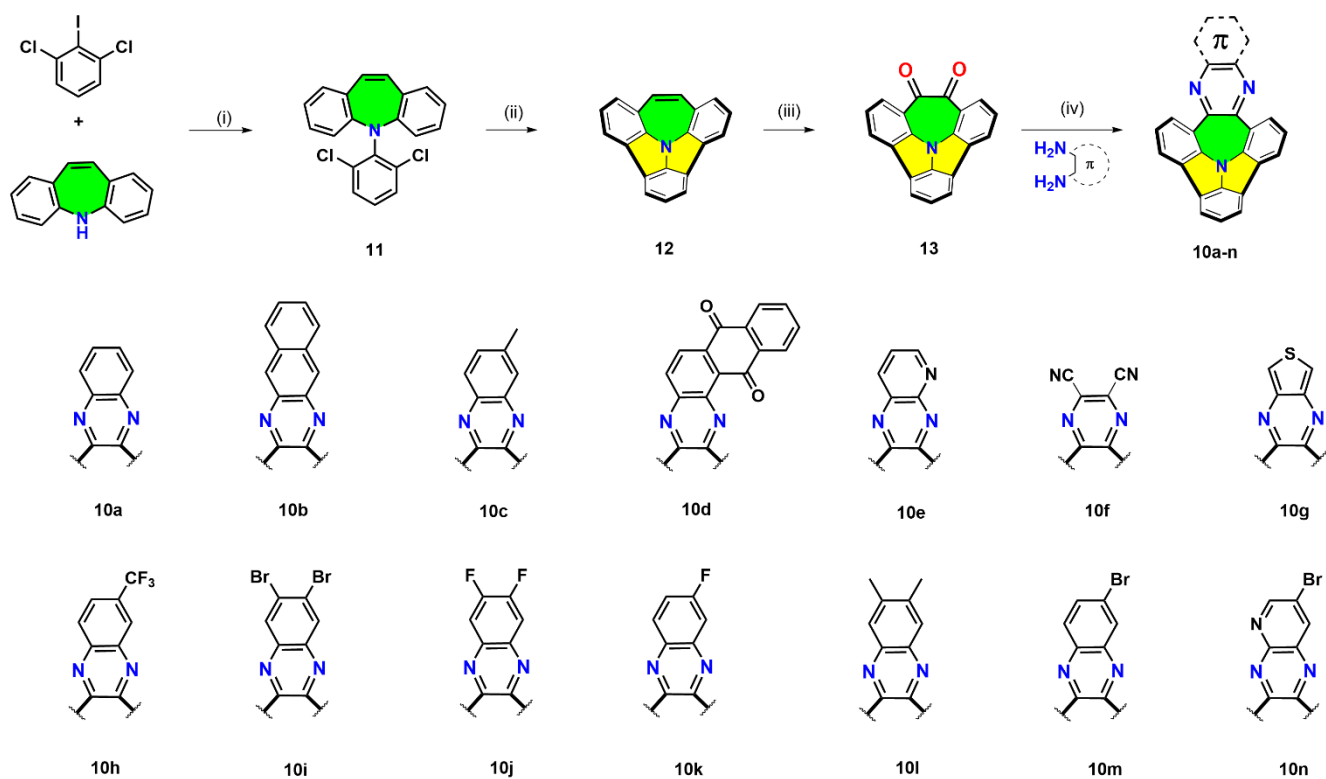
Figure 1. Chemical evolution of the N-doped PAHs

Non-planar species are formed when the N-dopant is partially or entirely encircled by pentagons and heptagons. Such structures have led to concave and bowl-shaped three-dimensional arrangements,^{12,13} a feature which significantly contributes to their photophysical properties.

In contrast to their planar analogs, relatively few examples of π -extended N-embedded PAHs (selected examples are shown in Figure 1b) have so far been reported as their preparation typically requires tedious and multi-step syntheses. Notably, seminal works on the pyrrole-embedded curved PAHs were independently reported by Nozaki and Shinokubo.^{18,19} Consecutively, Wang and co-workers demonstrated acridone (**6,7**)²⁰⁻²² and phenothiazine (**8**)²³ containing PAHs, as suitable building blocks to ensure the desired curvature for the construction of concave and boat-like conformations, respectively. Recently, the research group of Gryko showed the utility of pyrrolo[3,2-*b*]pyrrole in forming a bucky-bowl like system, with inverse Stone-Thrower-Wales defects, first through "on surface"²⁴ and subsequently "in solution"²⁵ approaches (Figure 1b, **9**). Despite the promising structural alignment of an electron-donating group (D), exploration of curved N-PAHs as prospective optoelectronic materials is limited by their relatively low emission efficiency. The tailoring of their bandgaps and S-T through modification of the periphery of the π -scaffold is the most straightforward method to optimize these properties. However, this approach is complicated by the need to attach solubilizing groups in what are often the most reactive positions of N-PAHs, which prevents further synthetic transformations with electron-accepting species (A). In part for this

reason, the rational design of nonplanar and thoroughly conjugated N-PAHs with a D-A electronic structure that compensates for the desired functions and synthetic availability has remained elusive.

The phenomenon of thermally activated delayed fluorescence (TADF) shows great promise for the enhancement of the external quantum efficiencies (EQEs) of organic light-emitting diodes (OLEDs). In principle at least, TADF-active organic emitters can quantitatively harvest the excitons generated in the emitting layer through electrical excitation, and convert them into light through efficient reverse intersystem crossing (rISC).²⁶⁻²⁹ The key issue in designing efficient TADF emitters is the acceleration of a spin-forbidden and endothermic rISC process ($T_1 \rightarrow S_1$). D-A π -conjugated systems with a sizeable D-A dihedral angle and vibrational motion achieve this by minimizing the singlet-triplet energy gap ($\Delta E_{ST} < 0.2$ eV) to lower the activation energy for rISC and mixing excited CT and LE states to allow spin-flip electronic transitions. Therefore, the development of TADF active organic materials has so far relied on planar and branched D-A species. A significant drawback of this architecture is that the radiative emission cross-sections are typically small. This effect adversely influences photoluminescence quantum yield (PLQY). On the other hand, when moderate ΔE_{ST} (0.3-0.6eV) is identified, in competition with TADF, photon emission through room-temperature phosphorescence (RTP)³⁰ can occur. Consequently, the molecular design targeted strictly at TADF or RTP is fundamentally important from the viewpoint of future applications in the



Reagents and conditions: (i) Pd(OAc)₂, P(tBu)₃HBF₄, NaOtBu, toluene; 89% (ii) [Pd(Pcy)₃]Cl₂, DBU, DMAc, MW, 77%; (iii) RuCl₃, NaIO₄, NMI, THF/DCM/H₂O, 37% or BSA *o*-dichlorobenzene, 65% (v) AcOH/EtOH, 1:1, 56-79%

Scheme 1 The synthetic path towards D-A arranged N-PAHs with an array of electronically diverse phenazines

domains of sensors, data encryption, and white-emitting OLEDs (WOLEDs).³¹

Herein, we report a concise and efficient synthetic strategy towards a new type of N-PAHs with intrinsic D-A electronic structures which are, for the first time, applied as yellow to orange TADF/RTP OLED emitters (Figure 1c). These compounds owe their attractive photophysical properties, such as the spatial separation of the HOMO and the LUMO, to an antiaromatic seven-membered ring located between the electron-donating and -accepting moieties. The entirely fused system has only moderate to weak oscillator strength (f) for HOMO \rightarrow LUMO transitions accompanied by a small $\Delta\epsilon_{S-T}$ energy. In contrast, the strength of the acceptor contributes to the remarkable PLQY amplification (up to 86%) determined for the most electron poor derivative. Thus, the OLEDs fabricated with the developed N-PAHs as TADF/RTP emitters can achieve an EQE as high as 12% along with satisfactory operational stability and a low roll-off process

Results and discussion

Molecular design and synthesis

To induce curvature in a PAH system, we devised a molecular design strategy that allowed two pentagons and one heptagon to be placed around a central nitrogen atom (Scheme 1). The synthetic pathway starts from the chemoselective Buchwald - Hartwig amination³⁴ of commercially available dibenz[*b,f*]azepine and 2,6-dichloro-1-iodobenzene delivering amine **11** in excellent 89% yield. Subsequent annulation of two 5-membered rings by microwave-assisted direct arylation was achieved through modification of Siegel's conditions³⁵ (only 5mol% of Pd-catalyst was implemented) in which the dichlorinated precursor was subjected to heating for 40 min to obtain compound **12** in 77% yield on a multigram scale. Inclusion of the unsaturated seven-membered ring of azepine³² in this structure allows for further oxidation to diketone **13**. The first oxidative approach we examined was that commonly used for the selective oxidation of pyrene-embedded PAHs.³⁶ Using this, the synthesis of the key intermediate **13** was achieved with an unsatisfying 37% yield. The use of benzeneseleninic acid anhydride (BSA)³⁷ proved significantly more effective, however, and the oxidation efficiency was raised to 65%. Such diones are known to readily undergo acid-promoted condensation with various 1,2-aromatic diamines to yield π -extended phenazines. Accordingly, a series of 14 phenazine derivatives (**10a-10n**) were created from appropriate diamines to give curved N-PAH derivatives with a range of electron acceptor properties and points of further functionalization.³³ Each synthetic step was found to be readily scalable, and three of them (see SI) could be performed without chromatographic separation which increases the prospective applicability of the current methodology. Incorporation of such a diverse range of fused phenazine derivatives with electronically varied substituents allows for strict control of the strength of the acceptor. With such molecular engineering, we anticipated that fine control of the optoelectronic features of our N-PAHs could be achieved with a great emphasis on excited states and bandgap energies.

Single-Crystal X-ray Crystallographic Analyses.

Single crystals of **10I** suitable for single crystal X-ray analysis were obtained by slow evaporation of a dichloromethane/tetrahydrofuran solvent mixture at room temperature. This compound crystallizes in the *P*-1 space group with two molecules in the unit cell. Analysis of the obtained structure, displayed in Figure 2, unambiguously confirmed the proposed concaved geometry. The distance of the central nitrogen atom and the plane of the three carbon atoms of the peripheral benzene rings indicate the depth to be 0.63 Å (Figure 2b). The three N-C bond lengths (see Fig. S8, SI) are in the range 1.36–1.38 Å, whereas the two newly formed C-C bond lengths are 1.48 Å, similar to those of analogous bonds in **6b** and **7** (1.49 Å).

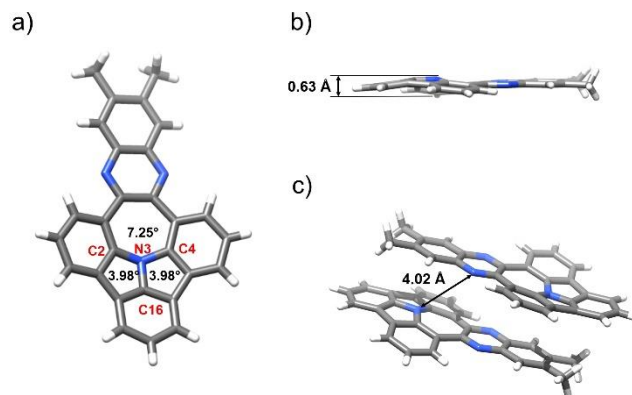


Figure 2. Crystal structure of **10I**; a) view of the crystal structure of **10I** from concave face and POAV angles; b) side view of the crystal structure of **10I** with measured depth; c) the molecular packing in the crystalline state

The less pronounced depth of **10I** compared to **6b** and **7** is due to the lower strain produced by the seven-membered ring in the N-PAHs reported here. This finding can be tracked with the π -orbital axis vector (POAV) angle (see Fig. 2b), that is a distinctive index for nonplanar compounds. In this consideration, the nitrogen POAV angle for **10I** (7.25°) was evaluated as to those of **5a/b** (\sim 7.55°),^{18,19} while fewer than for **6a/b**, **7** and **9** (15°-16.4°).^{20-22,25} Analogous deviation was measured for inner carbon atoms (C2, C4, C16) that occur in between 3.98°-5.25°. Interestingly, nearly all previously reported curved systems²⁰⁻²² stack in a concave-concave manner assembled in the same direction thus promoting undesirable π - π stacking (with the 3.17 Å distance between two adjacent molecules evidenced for **7**). Contrary to this, the obtained solid-state structure favors a “head-to-tail” antiperiplanar arrangement. As is shown in Fig 2c, tertiary amines are localized as opposed to each other with the almost parallel orientation of D-A units. This observation is manifested by short distances of 4.02 Å between nitrogen’s electron-rich and -deficient atoms. The predominant arrangement of neighboring molecules could favor the formation of excitons, which is beneficial from the viewpoint of photophysics and the further possible TADF/RTP OLED applications.

Quantum chemical calculations

The optical properties of **10a-10n** were first examined theoretically with the second-order algebraic diagrammatic construction theory with spin-component scaling (SCS-ADC(2)).^{38,39} For the sake of clarity, here we focus on **10l** as a representative example of this class of compounds. Calculation results for the other compounds are presented in the Supporting Information.

The calculated vertical excitation energies and associated oscillator strengths for **10l** are given in Table 1. Accompanying this data, in Figure 3 we show plots of natural transition orbitals (NTOs)⁴⁰ for transitions from the ground state into the two lowest singlets and the two lowest triplet excited states. According to our calculations, the lowest singlet excited state (S_1) of **10l** is a $\pi\pi^*$ -type state with a vertical excitation energy of 3.455 eV. Inspection of the predominant hole-particle NTO pair for the $S_0 \rightarrow S_1$ transition (Figure 3a) shows that the S_1 state has a partial charge-transfer character that arises from the excitation of an electron from a π orbital that is distributed mainly on rings VI, VII, and VIII into a π^* orbital that is localized on rings VII and VIII (see Figure 3 for the ring numbering). This transition is characterized by an appreciably large oscillator strength, considerably larger than the transitions into the other low-lying singlet excited states. Thus, the lowest photo-absorption band of **10l** can be assigned mainly to the transition into the S_1 state.

Table 1. Vertical excitation energies (ΔE) and associated oscillator strengths (f) of the representative compound **10l calculated at the SCS-ADC(2) level of theory. Calculations were performed at the ground-state equilibrium geometry optimized at the SCS-MP2 level.**

State	ΔE [eV]	f
S_1 ($1\pi\pi^*$)	3.455	0.3540
S_2 ($1\pi\pi^*$)	3.522	0.0361
S_3 ($1\pi\pi^*$)	3.870	0.0100
S_4 ($1n\pi^*$)	4.061	0.0033
T_1 ($3\pi\pi^*$)	2.984	0
T_2 ($3\pi\pi^*$)	3.091	0
T_3 ($3\pi\pi^*$)	3.398	0
T_4 ($3\pi\pi^*$)	3.419	0

The S_1 state is closely followed by the S_2 state with a vertical excitation energy of 4.522 eV. The S_2 state involves the excitation of an electron from a π orbital localized on rings II, III, IV, and V into a π^* orbital localized on rings I, II, III, IV, and V. The transition into the S_2 state displays a relatively low oscillator strength. Unlike the S_1 state, the S_2 state does not exhibit a significant charge-transfer character. The S_3 and S_4 states, in turn, are energetically well-separated from the S_1 and S_2 states, and display low oscillator strengths for transitions out of the ground state.

In the other compounds in the series **10a-10n**, the electronic structures of the S_1 and S_2 states are qualitatively similar as in **10l**. The exception is **10f**, for which the ordering of

the lowest two singlet states is inverted: in **10f**, the nearly dark $1\pi\pi^*$ state lies vertically below the bright $1\pi\pi^*$ state.

The lowest two triplet states (T_1 and T_2) are found at 2.984 eV and 3.091 eV, respectively. According to the NTO analysis, both states exhibit pronounced multiconfigurational character: that is to say, the $S_0 \rightarrow T_1$ and the $S_0 \rightarrow T_2$ transitions both have significant contributions from two hole-particle NTO pairs. This is presumably because the T_1 and T_2 states are close in energy and interact strongly with one another. We also located T_3 and T_4 states higher in energy, ca. 0.4 eV above the T_2 state.

In all cases, the first triplet state was found lower in energy than the first excited singlet state. However, the energy difference is rather small and yield on average 0.46 eV for the entire set. The lowest difference was identified for compound **10d** (0.24 eV).

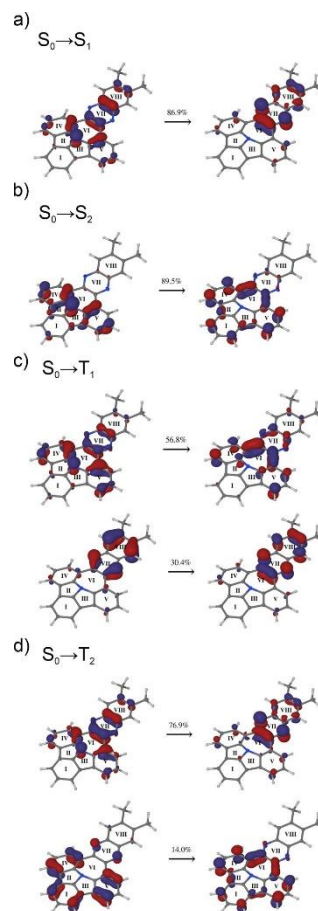


Figure 3 Dominant NTOs for vertical transitions of **10l** (SCS-ADC(2)) plotted as isosurfaces with isovalues of $\pm 0.05 a_0^{-3/2}$. The eigenvalue (λ_i) for each hole-particle NTO pair is given in terms of a percentage contribution. The rings are numbered with Roman numerals.

Photophysics

In the first step of optical measurements, the basic absorption and fluorescence spectra were collected to estimate the influence of structure on excitation and emission properties with respect to the electronic character of the acceptor (see

Figure 4). In all cases, we observed emission from the ^1LE in toluene, and from the ^1CT in more polar dichloromethane (DCM) and tetrahydrofuran (THF). Interestingly, there is no dramatic bathochromic shift related to the increase of polarity of the solvent. That could suggest mixed ^1LE and ^1CT character. The only significant shift was observed for the compound **10d** with the anthraquinone unit in DCM. As for the structural influence, there is a significant bathochromic shift of emission between **10a** and **10b**, related to the increase of conjugation in the structure due to the additional benzene ring. There is no significant influence by a methyl

group (**10c, 10l**), but the replacement of the phenazine electron-accepting moiety with an 1-azaphenazine moiety (**10e**) shifts the emission to lower energies (Figure 4). The highest bathochromic shift was observed due to the addition of two nitrile groups (**10f**). The impact of the halogen group is less impressive with the highest shift for double bromine atom side groups (**10i**), which is two times stronger than mono bromine substitution (**10m**). Similar behavior was observed for fluorine side groups (**10j, 10k**, Figure 4)).

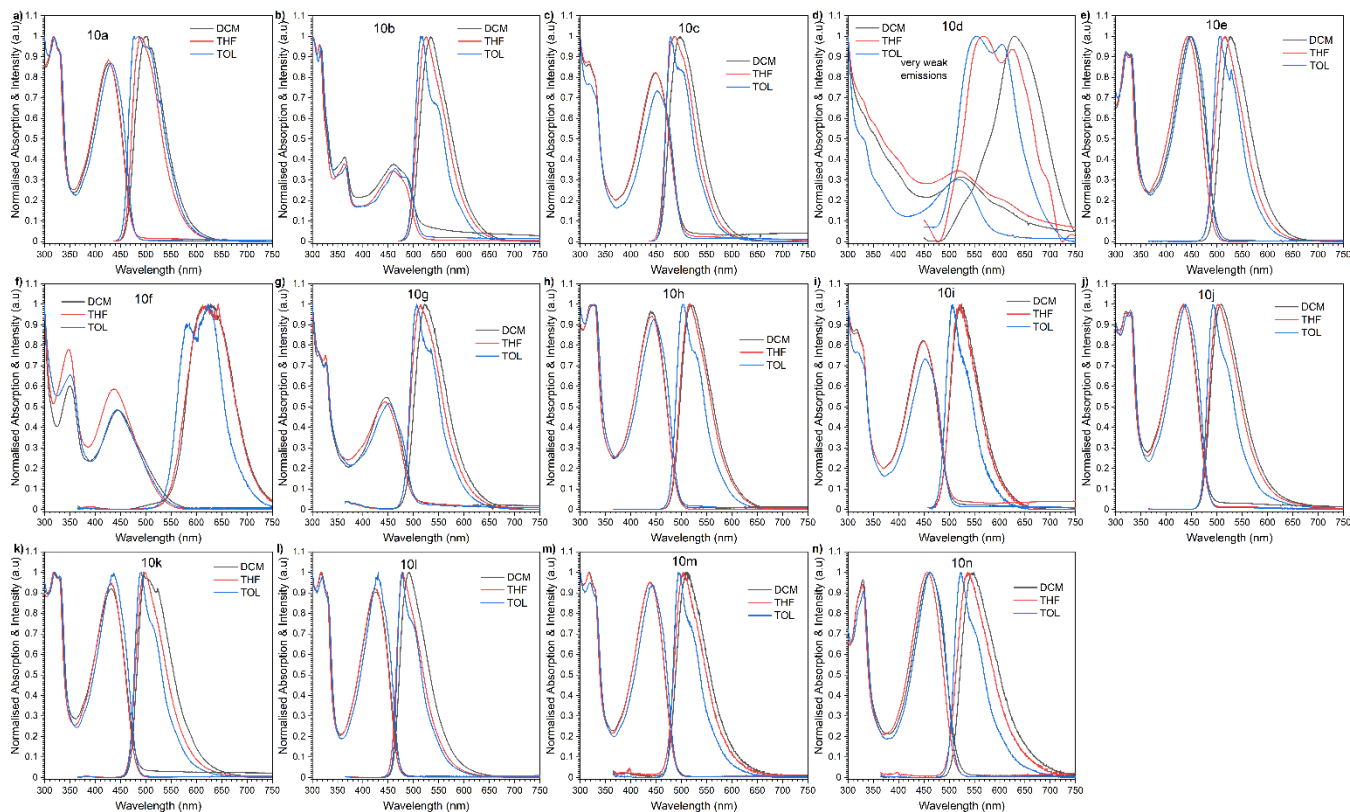


Figure 4. UV-vis absorption and PL spectra of **10a-n** (c 10^{-5} M) diluted solutions in dichloromethane, tetrahydrofuran, and toluene solvents.

As the next step, the synthesized compounds were investigated in the solid-state to gauge their potential as the active materials in organic light-emitting diode (OLED) structures. Two matrices were chosen to avoid possible aggregation, polymer Zeonex as the stage between solution and solid-state and 4,4'-bis(*N*-carbazolyl)-1,1'-biphenyl (CBP) as the host for OLEDs (Figure 5, Figure S2-S5, SI). For closer comparison we choose compounds **10b, d, f, g, h, m**, which present the most significant changes. It was noticed that the fluorescence emission (maximum peak) in the Zeonex matrix is similar to that in solutions (Figure 5). Depending on the substitution, thermally activated delayed fluorescence (TADF), room-temperature phosphorescence (RTP), or dual TADF & RTP were observed. Theoretically, to obtain efficient TADF emission, our compound should have as close as possible singlet and triplet excited states. There are several ways to estimate singlet and triplet excited states

including the onset of the respective emission or the maxima of the emissions. In our case, to allow for the comparison with theoretical calculations, we decide to use emission maxima. The lowest ΔE_{ST} gaps were observed for compounds with an additional benzene ring (**10b**), thiophene ring (**10g**) and double bromine substituents (**10i**) (Figure 5a, d, Table 2). In the two compounds **10b** and **10i**, the low ΔE_{ST} gap was connected with the same effect like in solution (an increase of conjugation, decrease the charge transfer energy). The groups affect the ^1CT energy state, where the triplet localized energy state remains (^3LE). In the case of the derivative with thiophene unit (**10g**), it seems that the group is affecting the triplet energy state, which is one of the highest (Figure 5d). To prove, which actual emission process is observed, the emission of the compounds at different delayed times were collected and compared (Figure S3, SI). Moreover, emission spectra were obtained at different

temperatures during the time-resolved photoluminescence measurement to estimate the location of phosphorescence and the point when thermal activation occurs. To decide if the compound exhibits emission through the TADF or RTP process, a comparison of ns range emission with at least μ s at 300 K and the phosphorescence emission is required. In our case, compounds **10d,g,h** had pure TADF emission, where delayed emission (80 ms, 300 K) matches the prompt ns emission (Figure 5b,d,e). If we look closely at the transient curves and inset spectra, it can be noticed that at microsecond delays, the spectra (Figure 5h,j,k) shift slightly to lower energies which is not so unusual in CT-based emitters and explained by local interactions between the dipole moment of the host and the excited state dipole moment of the

TADF molecule.⁴¹ In the case of **10b,f** we have mixed TADF&RTP emission where RTP contribution is higher than 1% (Figure 5a,c) but if we would look closely how the emission change at different delay times (Figure 5g,i) we would notice pure TADF emission at microsecond delay time which is important for OLED devices. The phosphorescence part starts to be visible above 1 ms delay time. From this set of compounds, only **10m** with a single bromine group had pure RTP emission at 80 ms delay time (Figure 5f), nevertheless, again if the microsecond range is checked, only pure TADF is observed which means in this case we have direct shift between TADF and RTP processes rather than dual emission (Figure 5l).

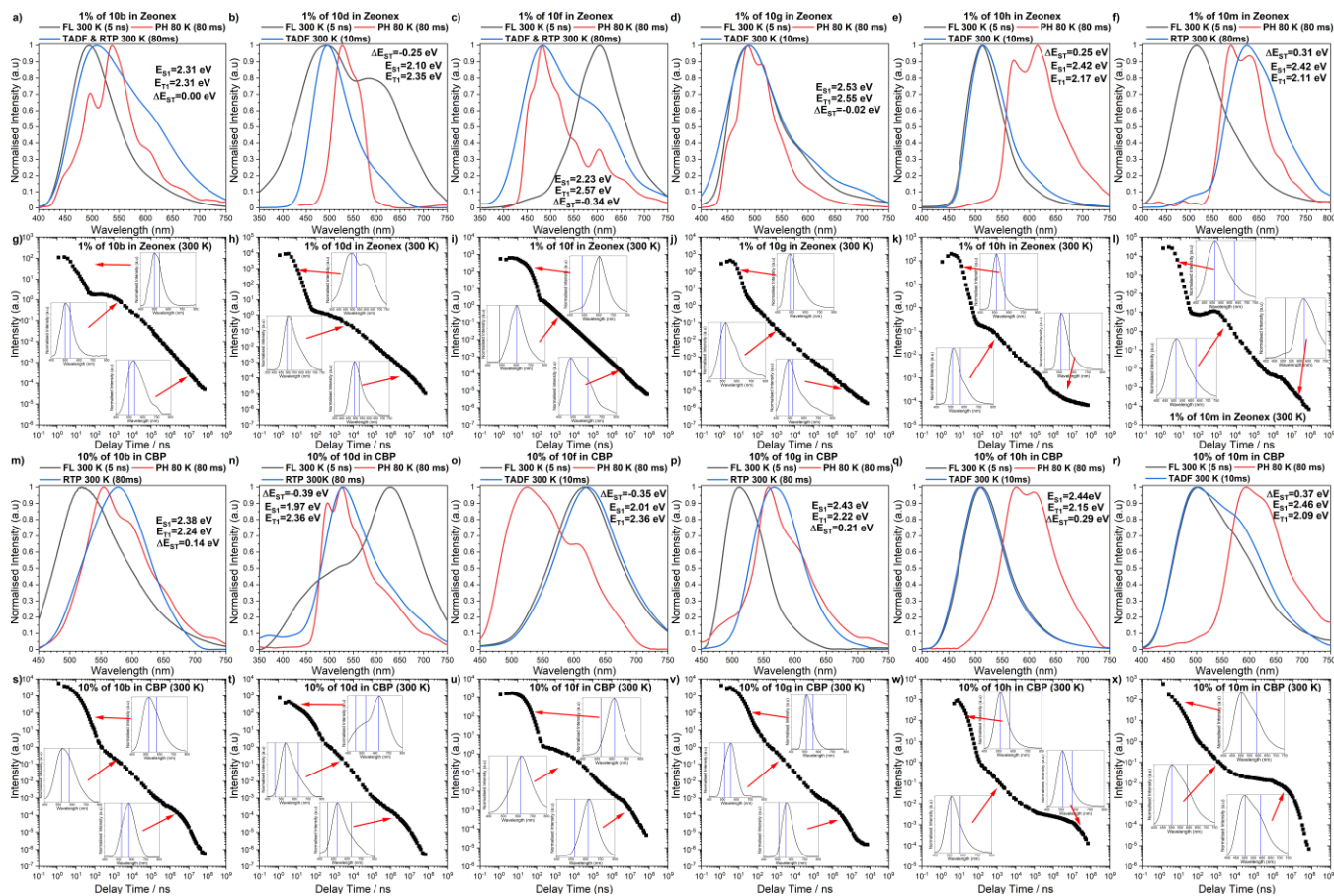


Figure 5. Time-Resolved Spectra of compounds **10b, d, f, g, h, m** in Zeonex (a-f) and CBP (m-r) matrix, the energies correspond to the maximum emission peaks. Intensity vs delay time measurement decays with the inset spectra collected at particular delay time of compounds in Zeonex (g-l)) and CBP matrix (s-x).

Nonetheless, the most intriguing behavior was observed for **10d** and **10f**. Insightful analysis of the obtained data hints at the appearance of an inversion of singlet and triplet energy states in both cases. In the case of **10d**, it may not be so obvious, but the prompt fluorescence emission is a set of two signals, one with maxima at 494 nm and the second at 590 nm. The signal at 494 disappears with a circa 10 ns delay time, and only the single emission at 590 nm remains. That means our lowest singlet state is 590 nm (2.10 eV) and our real $\Delta E_{ST} = -0.25$ eV (Figure 5b). A similar, but more

visible observation is identified for **10f**, for which the triplet energy state is 0.34 eV higher than the lowest singlet excited state (Figure 5c). It has to be noticed, however, that the experimental values are not in accordance with those extracted from ab-initio performed computations. The origin of negative ΔE_{ST} remains an open question and an additional, more targeted molecular design is indispensable to clearly elucidate the observed phenomena. Nevertheless, that is not all, in the case of **10d**, as delayed emission, we observe TADF but not from an S_1 energy state, but rather a

higher one (S_2). Such experimental finding is consistent with calculations (for more details see SI) made for compound **10d** as a significant f value ("bright" oscillator) for the S_2 state was determined.

In order to evaluate the potential of compounds **10a-10n** for application as materials for OLEDs, their photophysics was also characterized in the CBP matrix (see Figure 5 and Figures S4 and S5 in the Supporting Information). It turned out that changing the host matrix from Zeonex to CBP has a noticeable effect on their emission properties. Analyzing the emission in the CBP matrix, different properties can be noticed in comparison to Zeonex. Comparing emission at ms delay time, compounds **10f** and **10h** show pure TADF emission (Figure 5o,q), **10m** shows mixed emission (Figure 5r) and **10b,d,g** have RTP (Figure 5m,n,p), which in all but **10h** is completely different than in the Zeonex matrix. The matrix significantly affects **10d** containing anthraquinone and shifts it from mixed emission to RTP, but more interestingly, in both cases (Zeonex and CBP), the emission from the lowest state is not visible at longer delay times (Figure 5b,h,n,t). That means rISC process is blocked from passing to the lowest state but the excited state follows to a higher singlet state (Zeonex) or stays on the lowest triplet energy state (CBP). As for **10g**, the pure TADF in Zeonex changes to pure

RTP in CBP (Figure 5j,v). If we look at the respective energy levels (Table 2), for **10g**, both singlet and triplet energies are lowered, but the triplet state is more affected, increasing the ΔE_{ST} to 0.20 eV. This is enough for the TADF process to be turned off and RTP promoted. The process in **10b** is similar in CBP and Zeonex in the way that, if we look at the emission spectra development over delay time (Figure 5g,s), TADF emission starts to be visible in the μ s range and circles over the ISC/rISC process to ms delay times where the RTP process is involved. For compound **10b**, the shift from TADF to pure RTP is around 0.2 ms delay time (Figure 5s) where in the Zeonex matrix dual emission is observed (Figure 5a). For the other RTP emitters, **10d** and **10g**, the RTP is observed already at μ s delay times (Figure 5t,v), suggesting that it should work as RTP emitters in OLEDs. Similarly, to the Zeonex matrix, we could observe singlet-triplet inversion in the same two compounds (**10d** and **10f**), but the resulting effect is the opposite. In the case of **10d** in Zeonex, we observe TADF character, where in CBP, the emission shift to RTP (Figure 5h,t). In the **10f**, where in Zeonex we had dual TADF/RTP emission, in CBP, we observe pure TADF even at longest delay times (Figure 5i,u). For all compounds which had ΔE_{ST} in Zeonex close to 0, the gap significantly rose by at least 0.15 eV in CBP matrix (Table 2).

Table 2. Summary of the general photophysical properties of the compounds.

Compound	λ_{em} , nm ^a	Host	PLQY (%) ^b	τ_{PF} , ns ^c	τ_{DF} , μ s ^d	τ_{Ph} , ms ^d	DF/PF ^e	S_1 , eV ^f	T_1 , eV ^f	ΔE_{ST} , eV ^g
10a	493	Zeonex	10.3	3.89±0.15	10.81±0.94	1.80±0.10	1.01	2.51	2.23	0.28
	502	CBP	17.4	5.14±0.19	3.55±0.34	-	0.20	2.47	2.20	0.26
10b	536	Zeonex	35.8	5.22±0.37	1.82±0.12	9.23±0.83	21.49	2.31	2.31	0.00
	519	CBP	44.8	7.82±0.25	3.52±0.38	1.21±0.18	0.14	2.38	2.24	0.15
10c	497	Zeonex	8.4	4.96±0.23	2.47±0.12	5.97±0.57	2.80	2.50	2.20	0.30
	505	CBP	16.1	3.87±0.18	1.63±0.16	-	0.20	2.45	2.17	0.28
10d	497	Zeonex	1.7	3.04±0.04	7.43±0.65	-	0.46	2.10	2.35	-0.25
	456	CBP	16.2	15.68±0.91	2.42±0.30	-	0.43	1.97	2.36	-0.39
10e	519	Zeonex	36.4	6.95±0.38	4.30±0.49	-	8.17	2.39	2.17	0.22
	519	CBP	37.0	5.32±0.17	1.58±0.20	-	0.37	2.33	2.04	0.29
10f	555	Zeonex	6.2	25.42±1.12	0.94±0.06	-	0.35	2.23	2.57	-0.34
	617	CBP	86.4	23.74±1.14	1.00±0.09	-	1.89	2.01	2.36	-0.35
10g	490	Zeonex	2.0	4.73±0.38	0.96±0.08	-	0.38	2.53	2.55	-0.02
	511	CBP	29.3	7.80±0.17	0.58±0.02	0.72±0.07	0.18	2.43	2.22	0.20
10h	513	Zeonex	49.5	8.22±0.88	3.99±0.41	-	3.90	2.42	2.17	0.25
	507	CBP	36.7	9.41±0.24	1.60±0.11	-	5.30	2.44	2.15	0.29
10i	536	Zeonex	0.4	8.26±0.25	1.03±0.12	1.60±0.04	14.40	2.31	2.34	-0.03
	517	CBP	9.2	7.42±0.18	1.22±0.08	-	10.02	2.40	2.27	0.12
10j	525	Zeonex	18.1	10.02±0.42	2.78±0.37	-	3.05	2.36	2.07	0.29
	500	CBP	19.1	5.35±0.14	12.98±0.92	-	0.32	2.48	2.24	0.24
10k	511	Zeonex	16.7	7.74±0.75	1.20±0.13	-	3.06	2.42	2.13	0.29
	508	CBP	18.9	5.83±0.21	1.75±0.18	-	0.94	2.44	2.19	0.25
10l	495	Zeonex	12.4	3.10±0.13	0.66±0.05	6.70±0.73	4.36	2.50	2.18	0.32
	500	CBP	16.2	7.57±0.09	1.31±0.11	-	2.07	2.48	2.21	0.27
10m	512	Zeonex	1.0	3.07±0.31	1.58±0.14	3.12±0.23	0.73	2.42	2.11	0.31
	503	CBP	17.4	5.57±0.36	0.79±0.08	-	65.43	2.46	2.09	0.37
10n	546	Zeonex	2.1	4.05±0.02	1.98±0.18	-	13.14	2.12	2.04	0.08
	532	CBP	29.6	1.03±0.08	0.86±0.06	-	62.10	2.33	2.06	0.26

^a Photoluminescence maximum; ^b Photoluminescence quantum yield; ^c Prompt fluorescence lifetime in the host; ^d Delayed emission lifetime in the host; ^e Delayed fluorescence (DF) to prompt fluorescence (PF) ratio in the host; ^f Singlet and triplet energy in host. Error ± 0.03 eV; ^g Singlet-triplet energy splitting in Zeonex. Error ± 0.05 eV.

For the others, the change in the gap was much smaller and in the range of 0.05 eV to lower values. One of the most important factors describing the TADF impact on the final device is the DF/PF ratio, this factor tells us how much the triplet state contributes to the final emission. As it was stated by Dias et al.⁴¹ above 3 give us 100% use of generated triplets. In the Zeonex matrix, the **10b** compound showed the highest DF/PF (21.49, Table 2), nevertheless, above the threshold are also **10e,h,i,j,k,l,n**, which show the high impact of nitrogen insertion and halogen group to the rISC process. Unfortunately, in all cases but four (**10f,h,m,n**), we observe a decrease in the DF/PF ratio in the CBP matrix. In three (**10h,m,n**), the ratio is still above the threshold, and two (**10f,l**) at high value ca. 2. As for the RTP emitters (**10d,g**), in both cases, the overall RTP emission is much smaller than the fluorescence (0.43 and 0.18), (Table 2).

Fabrication and characterization of OLEDs devices

As the final stage, the OLED devices were fabricated and characterized (Figure 6). The behavior of the emitters in the CBP host was evaluated. The HOMO-LUMO values obtained from electrochemical measurement was used to evaluate the possible OLED device structures. The optimal device structure for the emitters was used in configuration: Devices **10a-n** -ITO/NPB [*N,N'*-di(1-naphthyl)-*N,N'*-diphenyl-(1,1'-biphenyl)-4,4'-diamine] (40 nm)/TSBPA [4,4'-(diphenylsilanediyl)bis(*N,N'*-diphenylaniline)] (10 nm)/10%

of **10a-n** in CBP (20 nm)/TPBi [2,2',2''-(1,3,5-benzinetriyl)-tris(1-phenyl-1-*H*-benzimidazole)] (50 nm)/LiF (1 nm)/Al (100 nm) (Figure 6). All the devices fabricated with the emitters except for **10d,g** showed electroluminescence which could be associated with TADF, whereas **10d** and **10g** had RTP emission, which is supported by photophysical analysis. The characteristics of the OLED devices revealed a significant increase in OLED efficiency depending on the structure (Figure 6b,e). The device based on emitter **10h** with the trifluoromethyl group was found to be the most efficient with external quantum efficiency around 12% (Figure 6b). Also, about 10% EQE was obtained for the device based on emitter **10f** with double nitrile groups and singlet-triplet inversion effect. The highest RTP based OLED was obtained for devices based on emitter **10g** with thiophene unit, up to 3%. The highest luminance was obtained for the OLED based on emitter **10f**, with up to 24,680 cd/m², whereas for the RTP based OLED (**10g**), up to 10,250 cd/m² was recorded (Figure 6c). If we think about the molecular structure impact on the final device, the additional benzene ring allows the EQE to increase by 2.5 times (**10a, 10b**). The insertion of the nitrogen group resulted in doubling of EQE (**10a, 10e**) and quadrupling with the addition of a bromine group (**10a, 10n**). Pure halogen groups had only a limited impact on the increase of the overall efficiency (lower than 2x).

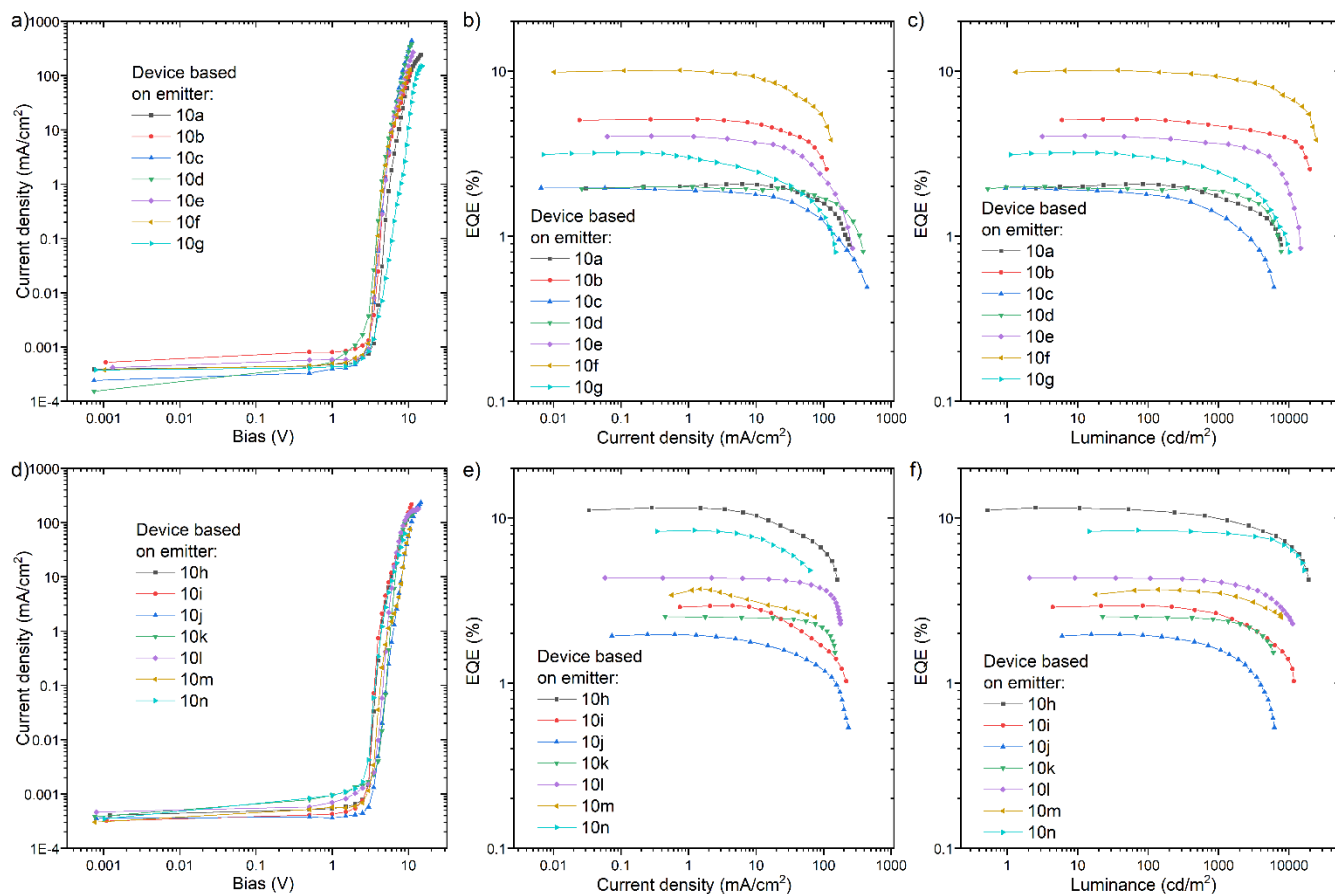


Figure 6. The characteristics of the OLED devices based on emitters **10a-n**. a), d) Current density-bias characteristics. b), e) EQE-current density characteristics. c), f) EQE - luminance characteristics.

Conclusions

We have successfully synthesized a large family of unique, phenazine terminated aza-bowled polycyclic aromatic hydrocarbons which were identified as an interesting group of novel emitters. These display a curvature that was unambiguously confirmed by X-ray crystallographic analysis which also revealed desirable intermolecular D \cdots A interactions. Further examination of physicochemical properties, in conjunction with quantum calculations, highlighted the effect the phenazine side group has on the emission properties. Through modulation of the strength of this phenazine acceptor, excellent photoluminescence quantum yields (up to 86%) could be achieved in addition to a controlled change between thermally activated delayed fluorescence (TADF) or room-temperature phosphorescence (RTP). The N-PAHs were incorporated into OLEDs and the largest output among all fabricated devices was from the emitter containing a dinitrile terminated species, resulting in a very high efficiency (>11%) and a very efficient TADF process. These studies provided a new, conceptually simple, and synthetically affordable, route towards D-A curved N-PAHs systems with excellent optoelectronic properties which were utilized as functional materials. The strategy established here opens an avenue for tuning the photo and redox properties of non-planar N-PAHs through rational vertical and/or horizontal synthetic modifications. This approach could also potentially lead to compounds which exhibit singlet-triplet inversion, which is an ongoing field of research in our laboratory.

ASSOCIATED CONTENT

This material is available free of charge via the Internet at <http://pubs.acs.org>.

Accession Code CCDC 2128847 contains the supplementary crystallographic data for this paper. These data can be obtained free of charge via www.ccdc.cam.ac.uk/data_request/cif, or by emailing data_request@ccdc.cam.ac.uk, or by contacting The Cambridge Crystallographic Data Centre, 12 Union Road, Cambridge CB2 1EZ, UK; fax: +44 1223 336033.

AUTHOR INFORMATION

Corresponding Author

* Adam Kubas - Institute of Physical Chemistry, Polish Academy of Sciences, Kasprzaka 44/52, 01-224 Warsaw, Poland; <https://orcid.org/0000-0002-5508-0533>; akubas@ichf.edu.pl

* Przemysław Data - Silesian University of Technology, Faculty of Chemistry, Department of Physical Chemistry and Technology of Polymers, Strzody 9/208d, 44-100 Gliwice, Poland; <https://orcid.org/0000-0002-1831-971X>, przemyslaw.data@polsl.pl

* Marcin Lindner - Institute of Organic Chemistry, Polish Academy of Sciences, Kasprzaka 44/52, 01-224 Warsaw, Poland; <https://orcid.org/0000-0002-5514-674X>; mlindner@icho.edu.pl

Authors

Jakub Wagner - Institute of Organic Chemistry, Polish Academy of Sciences, Kasprzaka 44/52, 01-224 Warsaw, Poland; <https://orcid.org/0000-0002-7754-2014>; jwagner@icho.edu.pl

Paola Zimmermann Crocomo - Silesian University of Technology, Faculty of Chemistry, Department of Physical Chemistry and Technology of Polymers, Strzody 9/208d, 44-100 Gliwice, Poland; <https://orcid.org/0000-0002-1831-971X>, paola.crocomo@polsl.pl

Michał Andrzej Kochman - Institute of Physical Chemistry, Polish Academy of Sciences, Kasprzaka 44/52, 01-224 Warsaw, Poland; <https://orcid.org/0000-0003-2552-9464>; mkochman@ichf.edu.pl

Author Contributions

†J.W., J.Z.C., M.A.K. contributed equally

Funding Sources

National Science Centre, Poland, Grant No. UMO-2018/31/D/ST5/00426

National Science Centre, Poland, Grant No. 2020/39/B/ST4/01952

EU H2020 MSCA grant agreement No. 847413

Minister of Science and Higher Education of Poland "PMW" program agreement no. 5005/H2020-MSCA-COFUND/2019/2 Polish National Science Centre funding, grant no. 2017/25/B/ST5/02488.

EU H2020 ERA-Chair project ExCEED, grant agreement No 952008.

Notes

The authors declare no competing financial interest.

ACKNOWLEDGMENT

J.W. and M.L. acknowledge support from the National Science Centre, Poland, Grant No. UMO-2018/31/D/ST5/00426

M.L. is a recipient of a scholarship awarded by the Polish Ministry of Education and Science to outstanding young scientists.

M. A. K. acknowledges funding from the European Union's Horizon 2020 research and innovation program under the Marie Skłodowska-Curie grant agreement No. 847413. A. K. acknowledges support from the National Science Centre, Poland, Grant No. 2020/39/B/ST4/01952.

This work has been published as part of an international co-financed project funded from the program of the Minister of Science and Higher Education entitled "PMW" in the years 2020–2024; agreement no. 5005/H2020-MSCA-COFUND/2019/2. The electronic structure calculations reported in this study were carried out with the use of the computational resources provided by Wrocław Centre for Networking and Supercomputing (WCSS, <http://wcss.pl>) and the Centre of Informatics of the Tricity Academic Supercomputer and Network (CI TASK, <https://task.gda.pl/>).

P.D. and P.Z.C. acknowledges the Polish National Science Centre funding, grant no. 2017/25/B/ST5/02488. P.D. and P.Z.C. acknowledges the supporting awards from the Rector of the Silesian University of Technology (04_040_SDU_10-22-04, 04/040/RGJ21/0149). P.D. and P.Z.C. acknowledges the supporting actions from EU's Horizon 2020 ERA-Chair project ExCEED, grant agreement No 952008. We gratefully acknowledge the generous support from these agencies.

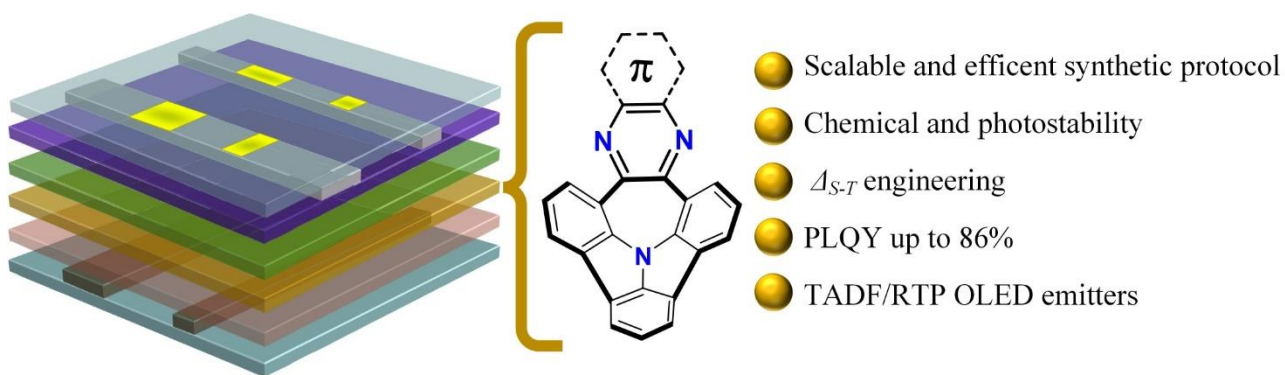
We are grateful to Mr Jan-Simon von Glasenapp of the Otto Diels-Institute for Organic Chemistry at the Christian-Albrechts-University of Kiel for providing us with a copy of the ACID software package and helpful instructions on compiling and using that program.

The authors thank to Dr Krzysztof Bartkowski (IOC PAS) and Dr. David C. Young for proofreading the manuscript.

REFERENCES

- (1) Narita, A.; Wang, X.-Y.; Feng, X.; Müllen, K. New Advances in Nanographene Chemistry. *Chemical Society Reviews* **2015**, *44* (18), 6616–6643.
- (2) Stępień, M.; Gońka, E.; Żyła, M.; Sprutta, N. Heterocyclic Nanographenes and Other Polycyclic Heteroaromatic Compounds: Synthetic Routes, Properties, and Applications. *Chemical Reviews* **2017**, *117* (4), 3479–3716.
- (3) Borissov, A.; Maurya, Y. K.; Moshniaha, L.; Wong, W.-S.; Żyła-Karwowska, M.; Stępień, M. Recent Advances in Heterocyclic Nanographenes and Other Polycyclic Heteroaromatic Compounds. *Chemical Reviews* **2021**, *acs.chemrev.1c00449*; doi.org/10.1021/acs.chemrev.1c00449.
- (4) Bachar, N.; Liberman, L.; Muallem, F.; Feng, X.; Müllen, K.; Haick, H. Sensor Arrays Based on Polycyclic Aromatic Hydrocarbons: Chemiresistors versus Quartz-Crystal Microbalance. *ACS Applied Materials & Interfaces* **2013**, *5* (22), 11641–11653.
- (5) Miao, Q. Ten Years of N-Heteropentacenes as Semiconductors for Organic Thin-Film Transistors. *Advanced Materials* **2014**, *26* (31), 5541–5549.
- (6) Aumaitre, C.; Morin, J. Polycyclic Aromatic Hydrocarbons as Potential Building Blocks for Organic Solar Cells. *The Chemical Record* **2019**, *19* (6), 1142–1154.
- (7) Hong, G.; Diao, S.; Antaris, A. L.; Dai, H. Carbon Nanomaterials for Biological Imaging and Nanomedical Therapy. *Chemical Reviews* **2015**, *115* (19), 10816–10906.
- (8) Weil, T.; Vosch, T.; Hofkens, J.; Peneva, K.; Müllen, K. The Rylene Colorant Family-Tailored Nanoemitters for Photonics Research and Applications. *Angewandte Chemie International Edition* **2010**, *49* (48), 9068–9093.
- (9) Jung, C.; Müller, B. K.; Lamb, D. C.; Nolde, F.; Müllen, K.; Bräuchle, C. A New Photostable Terrylene Diimide Dye for Applications in Single Molecule Studies and Membrane Labeling. *Journal of the American Chemical Society* **2006**, *128* (15), 5283–5291.
- (10) Schmidt-Mende, L.; Fechtenkötter, A.; Müllen, K.; Moons, E.; Friend, R. H.; MacKenzie, J. D. Self-Organized Discotic Liquid Crystals for High-Efficiency Organic Photovoltaics. *Science* **2001**, *293* (5532), 1119–1122.
- (11) Klaus Müllen; Ullrich Scherf. *Organic Light Emitting Devices: Synthesis, Properties and Applications*. Wiley-VCH: Weinheim, 2006.
- (12) Hirai, M.; Tanaka, N.; Sakai, M.; Yamaguchi, S. Structurally Constrained Boron-, Nitrogen-, Silicon-, and Phosphorus-Centered Polycyclic π -Conjugated Systems. *Chemical Reviews* **2019**, *119* (14), 8291–8331.
- (13) Schaub, T. A.; Padberg, K.; Kivala, M. Bridged Triarylboranes, -silanes, -amines, and -phosphines as Minimalistic Heteroatom-containing Polycyclic Aromatic Hydrocarbons: Progress and Challenges. *Journal of Physical Organic Chemistry* **2020**, *33* (2).
- (14) Kuratsu, M.; Kozaki, M.; Okada, K. 2,2':6',2'':6'',6-Trioxyltriphenylamine: Synthesis and Properties of the Radical Cation and Neutral Species. *Angewandte Chemie - International Edition* **2005**, *44* (26), 4056–4058.
- (15) Gilman, H.; Stuckwisch, C. G. The Di-Metalation of 9-Phenylcarbazole. *Journal of the American Chemical Society* **1943**, *65* (9), 1729–1733.
- (16) Kato, S. ichiro; Matsuoka, T.; Suzuki, S.; Asano, M. S.; Yoshihara, T.; Tobita, S.; Matsumoto, T.; Kitamura, C. Synthesis, Structures, and Properties of Neutral and Radical Cationic s,c,c-Bridged Triphenylamines. *Organic Letters* **2020**, *22* (2), 734–738.
- (17) Zou, S. N.; Peng, C. C.; Yang, S. Y.; Qu, Y. K.; Yu, Y. J.; Chen, X.; Jiang, Z. Q.; Liao, L. S. Fully Bridged Triphenylamine Derivatives as Color-Tunable Thermally Activated Delayed Fluorescence Emitters. *Organic Letters* **2021**, *23* (3), 958–962.
- (18) Ito, S.; Tokimaru, Y.; Nozaki, K. Benzene-Fused Azacoronulene Bearing an Internal Nitrogen Atom. *Angewandte Chemie International Edition* **2015**, *54* (25), 7256–7260.
- (19) Yokoi, H.; Hiraoka, Y.; Hiroto, S.; Sakamaki, D.; Seki, S.; Shinokubo, H. Nitrogen-Embedded Buckybowl and Its Assembly with C60. *Nature Communications* **2015**, *6* (1), 8215–.
- (20) Deng, N.; Zhang, G. Nitrogen-Centered Concave Molecules with Double Fused Pentagons. *Organic Letters* **2019**, *21* (13), 5248–5261.
- (21) Song, Y.; Zhang, G. Effect of Fusion Manner of Concave Molecules on the Properties of Resulting Nanoboats. *Organic Letters* **2021**, *23* (2), 491–496.
- (22) Zhou, L.; Zhang, G. A Nanoboat with Fused Concave N-Heterotriangulene. *Angewandte Chemie - International Edition* **2020**, *59* (23), 8963–8968.
- (23) Zhu, G.; Song, Y.; Zhang, Q.; Ding, W.; Chen, X.; Wang, Y.; Zhang, G. Modulating the Properties of Buckybowls Containing Multiple Heteroatoms. *Organic Chemistry Frontiers* **2021**, *8* (4), 727–735.
- (24) Mishra, S.; Krzeszewski, M.; Pignedoli, C. A.; Ruffieux, P.; Fasel, R.; Gryko, D. T. On-Surface Synthesis of a Nitrogen-Embedded Buckybowl with Inverse Stone-Thrower-Wales Topology. *Nature Communications* **2018**, *9* (1), 1714.
- (25) Krzeszewski, M.; Dobrzycki, Ł.; Sobolewski, A. L.; Cyrański, M. K.; Gryko, D. T. Bowl-Shaped Pentagon- and Heptagon-Embedded Nanographene Containing a Central Pyrrolo[3,2-b]Pyrrole Core. *Angewandte Chemie - International Edition* **2021**, *60* (27), 14998–15005.
- (26) Yang, Z.; Mao, Z.; Xie, Z.; Zhang, Y.; Liu, S.; Zhao, J.; Xu, J.; Chi, Z.; Aldred, M. P. Recent Advances in Organic Thermally Activated Delayed Fluorescence Materials. *Chemical Society Reviews* **2017**, *46* (3), 915–1016.
- (27) Wong, M. Y.; Zysman-Colman, E. Purely Organic Thermally Activated Delayed Fluorescence Materials for Organic Light-Emitting Diodes. *Advanced Materials* **2017**, *29* (22), 1605444.
- (28) Chen, X.-K.; Kim, D.; Brédas, J.-L. Thermally Activated Delayed Fluorescence (TADF) Path toward Efficient Electroluminescence in Purely Organic Materials: Molecular

- Level Insight. *Accounts of Chemical Research* **2018**, *51* (9), 2215–2224.
- (29) Liu, Y.; Li, C.; Ren, Z.; Yan, S.; Bryce, M. R. All-Organic Thermally Activated Delayed Fluorescence Materials for Organic Light-Emitting Diodes. *Nature Reviews Materials* **2018**, *3* (4), 18020.
- (30) Data, P.; Takeda, Y. Recent Advancements in and the Future of Organic Emitters: TADF- and RTP-Active Multifunctional Organic Materials. *Chemistry – An Asian Journal* **2019**, *14* (10), 1613–1636.
- (31) Kukhta, N. A.; Bryce, M. R. Dual Emission in Purely Organic Materials for Optoelectronic Applications. *Materials Horizons* **2021**, *8* (1), 33–55.
- (32) Kricka, L. J.; Ledwith, A. Dibenz[b,f]Azepines and Related Ring Systems. *Chemical Reviews* **1974**, *74* (1), 101–123.
- (33) Wu, Y.; Jin, Y.; Xu, J.; Lv, Y.; Yu, J. Recent Progress in the Synthesis and Applications of Azaacenes. *Current Organic Chemistry* **2020**, *24* (8), 885–899.
- (34) Surry, D. S.; Buchwald, S. L. Dialkylbiaryl Phosphines in Pd-Catalyzed Amination: A User's Guide. *Chem. Sci.* **2011**, *2* (1), 27–50.
- (35) Steinberg, B. D.; Jackson, E. A.; Filatov, A. S.; Wakamiya, A.; Petrukhina, M. A.; Scott, L. T. Aromatic π -Systems More Curved Than C_{60} . The Complete Family of All Indenocorannulenes Synthesized by Iterative Microwave-Assisted Intramolecular Arylations. *Journal of the American Chemical Society* **2009**, *131* (30), 10537–10545.
- (36) Hu, J.; Zhang, D.; Harris, F. W. Ruthenium(III) Chloride Catalyzed Oxidation of Pyrene and 2,7-Disubstituted Pyrenes: An Efficient, One-Step Synthesis of Pyrene-4,5-Di-ones and Pyrene-4,5,9,10-Tetraones. *The Journal of Organic Chemistry* **2005**, *70* (2), 707–708.
- (37) G. Back, T. Oxidations Catalyzed By Seleninic Acids and Anhydrides, Their Precursors and Congeners. *Current Green Chemistry* **2016**, *3* (1), 76–91.
- (38) Trofimov, A. B.; Schirmer, J. An Efficient Polarization Propagator Approach to Valence Electron Excitation Spectra. *Journal of Physics B: Atomic, Molecular and Optical Physics* **1995**, *28* (12), 2299–2324.
- (39) Köhn, A.; Hättig, C. Analytic Gradients for Excited States in the Coupled-Cluster Model CC2 Employing the Resolution-of-the-Identity Approximation. *Journal of Chemical Physics* **2003**, *119* (10).
- (40) Martin, R. L. Natural Transition Orbitals. *Journal of Chemical Physics* **2003**, *118* (11), 4775.
- (41) Dias, F. B.; Penfold, T. J.; Monkman, A. P. Photophysics of Thermally Activated Delayed Fluorescence Molecules. *Methods and Applications in Fluorescence*. 2017. 5, 012001



TADF/RTP OLED

Insert Table of Contents artwork here
